INTERNATIONAL JOURNAL FOR NUMERICAL METHODS IN FLUIDS
Int. J. Numer. Meth. Fluids 2001; **35**: 559–573

Numerical simulation of White–Metzner fluid in a 4:1 contraction

S. Raghay* and A. Hakim

Département de Mathematiques et Informatique, Faculté des Sciences et Techniques, Marrakech, Morocco

SUMMARY

A finite volume technique has been introduced in an attempt to simulate a viscoelastic flow. The steady flow of a White–Metzner fluid through a 4:1 abrupt contraction has been chosen as a prototype example because of the existence of previous simulations in the literature. The finite volume method (FVM) is used to discretize the conservation and constitute equations with a Hybrid scheme with appropriate treatment of source terms. The FVM is proven to be quite capable of handling numerically viscoelastic models with low computational cost. Its use is recommended as a viable alternative to the solution of viscoelastic problems using a variety of constitutive models. Copyright © 2001 John Wiley & Sons, Ltd.

KEY WORDS: finite volume; non-uniform staggered grid; numerical simulation; planar contraction; viscoelastic flows; White–Metzner model

1. INTRODUCTION

For the past several years, numerical simulation of viscoelastic flows has been a powerful tool for understanding the fluid behaviour in a variety of processes of both industrial and scientific interest. Polymeric fluids, owing to their viscoelastic character, are of particular interest in numerical simulations because of their wide applications in material processing and their behaviour is different from that of Newtonian fluids in ways which are often complex and striking. Although, there have been many successful numerical complexities that arise due to the change of type, i.e. hyperbolic–elliptic or hyperbolic–parabolic. The earlier numerical schemes, such as central finite differences [1–3], Galerkin finite elements [4] and spectral finite elements [5], to solve the equations are unstable when the elasticity of the flow becomes significant. While each of them has its advantages and disadvantages, the search for even better and/or faster methods still continues. In that respect, it was inevitable that the FVM should also be tried within the viscoelastic context. However, the viscoelastic simulations with the FVM are very limited [12–16].

* Correspondence to: Département de Mathematiques et Informatique, Faculté des Sciences et Techniques, Université Cadi Ayyad FSTG, BP 618, Gueliz, Marrakech, Morocco.

Received July 1999
Revised February 2000

Contraction flows of viscoelastic fluids are of importance in fundamental flow property measurements as well as in many industrial applications involving moulding and extrusion of polymer melts and solutions. They are also a challenging class of problems for analytical and numerical work. Numerous theoretical studies have been devoted to the study of viscoelastic fluids in contraction flow and there is a large literature on this subject; see, for example, References [6,7]. However, the theoretical prediction of entry-flow for non-Newtonian fluids remains a different task. The constitutive equation used to describe the rheology of the polymer has fading memory effects, and may contain non-linear terms that add to the complexity of the problem. The presence of a geometrical singularity poses another major challenge to the numerical simulation of contraction flows.

Even though polymer melts and solutions are rheologically difficult to study in complex flow geometries, many studies have been devoted to this topic. In particular, a large number of articles on numerical studies of polymer solutions in contraction flows exist. Maders *et al.* [8] used a decoupled finite element method to simulate the White–Metzner fluid flow. They showed that no loss of evolution has been observed until a Weissenberg number $We = 1.85$. They conducted a numerical simulation for a 4:1 contraction flow for comparison with the experimental results. They reported satisfactory agreement between experiments and computations at low flow rates, even if the experimental first principal stress difference relaxes more rapidly in the downstream region than the computed one. In spite of the numerous works that have tried to compare theoretical and experimental results, there is still a need for more extensive studies that examine all aspects of the flow at different locations of the geometry, and establish a systematic comparison between experimental and numerical calculations.

In this paper we conduct a numerical simulation of the planar contraction flow of viscoelastic fluid (see Figure 1 for computational domain of the 4:1 contraction). Since the nature of the rheological constitutive low used to describe the polymer solution will influence the predictions, we used the White–Metzner model, which generalizes many rheological models.

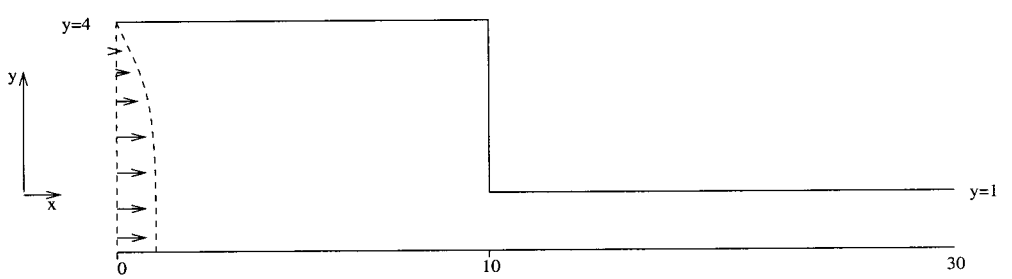

Figure 1. Computational domain for contraction flow.

2. GOVERNING EQUATIONS

For the two-dimensional flow of an incompressible viscoelastic fluid, the governing equations are continuity, the x and y component momentum equations, and three component stress equations from the constitutive equation. The solution of these equations, with appropriate boundary conditions, gives u, v, τ_{xx}, τ_{yy}, τ_{xy}, and the pressure p as functions of x and y. The equations expressed below are in terms of dimensionless variables.

$$\begin{cases} Re(u\cdot\nabla)u + \nabla P = (1 - w_r)\Delta u + \nabla\cdot\tau + f \\ \operatorname{div} u = 0 \\ \dfrac{\tau}{\lambda_{II}} + (u\cdot\nabla)\tau + \beta(\tau, \nabla u) = 2w\mu_{II}D \end{cases}$$

where

$$\beta(\tau, \nabla u) = 2\varepsilon[D\cdot\tau + \tau\cdot D] - [(\nabla u)\tau + \tau(\nabla u)^t]$$

$$D = \frac{1}{2}(\nabla u + (\nabla u)^T)$$

$$\lambda_{II} = We\,\frac{\sigma}{[1 + 4\varepsilon(1-\varepsilon)We^2 II]^{\beta}}$$

$$\eta_{II} = \frac{1 + 4\varepsilon(1-\varepsilon)\lambda_{II}^2 II}{[1 + 4\varepsilon(1-\varepsilon)We^2 II]^{\alpha}}$$

$$II = \frac{1}{2}\left[\left(\frac{\partial u}{\partial x}\right)^2 + \left(\frac{\partial v}{\partial y}\right)^2 + \frac{1}{2}\left(\frac{\partial u}{\partial y} + \frac{\partial v}{\partial x}\right)^2\right]$$

2.1. Boundary conditions

The boundary conditions employed for the velocity and pressure are given below:

In inlet and outlet section fully developed Poiseuille flow is imposed

$$\begin{cases} u(0, y) = \dfrac{3}{2}U_m\left(1 - \left(\dfrac{y}{4}\right)^2\right), & v(0, y) = 0 \\ u(L, y) = \dfrac{3}{2}U_v(1 - y^2), & v(L, y) = 0 \end{cases}$$

where $U_v = \frac{1}{3}$ and $U_m = U_v/4$.

The extra stress components are fixed along the inlet section. They correspond to a fully developed flow of a White–Metzner fluid between parallel plates

$$\begin{cases} \tau_{xx} = 18 w_r We \left(\dfrac{U_m}{4}\right)^2 \left(\dfrac{y}{4}\right)^2 \\ \tau_{xy} = -3 w_r We \dfrac{U_m}{4} \dfrac{y}{4} \\ \tau_{yy} = 0 \end{cases}$$

at the centreline we impose symmetry conditions

$$\frac{\partial u}{\partial y}(x, 0) = 0, \qquad v(x, 0) = 0$$

and adhesion at the wall:

$$u = 0, \qquad v = 0$$

3. NUMERICAL METHOD

To solve the above coupled non-linear equations at moderate cost, the use of an iterative numerical method has to be made. The mathematical analysis of these equations is studied by Reference [9]. It has to be noticed that all of the governing equations can be written in the form of general transport equation as follows

$$\frac{\partial}{\partial x_j}\left(\Lambda u_j \Phi - \Gamma \frac{\partial \Phi}{\partial x_j}\right) = S_\Phi \tag{1}$$

where Φ is the working variable which can be a component of a vector or tensor and even a constant. The coefficients Λ and Γ have different meanings for different equations, and S_Φ is called the source term, which includes all the terms that cannot be taken into account in the convective and diffusion terms, and has different contents for different equations. These variables are given in Table I. A simple finite volume formulation is used for the spatial discretization. The flow domain is divided into a set of control volumes ΔV around P, with bounding area A as shown in Figure 2.

Integrating Equation (1) over the control volume and using the divergence theorem, we have

$$\int \left(\Lambda u_j \Phi - \Gamma \frac{\partial \Phi}{\partial x_j}\right) n_j \, \mathrm{d}A = \bar{S}_\Phi \tag{2}$$

where $\bar{S}_\Phi$ is the integral of the source term S_Φ. This can be linearized as

Table I. Variables.

Φ	Λ	Γ	S_Φ
1	1	—	0
u	Re	$1-w_r$	$-\dfrac{\partial p}{\partial x}+\dfrac{\partial \tau_{xx}}{\partial x}+\dfrac{\partial \tau_{xy}}{\partial y}$
v	Re	$1-w_r$	$-\dfrac{\partial p}{\partial y}+\dfrac{\partial \tau_{xy}}{\partial x}+\dfrac{\partial \tau_{yy}}{\partial y}$
τ_{xx}	1	0	$-\varepsilon\left(2\tau_{xx}\dfrac{\partial u}{\partial x}+\tau_{xy}\left(\dfrac{\partial u}{\partial y}+\dfrac{\partial u}{\partial x}\right)\right)+2\left(\tau_{xx}\dfrac{\partial u}{\partial x}+\tau_{xy}\dfrac{\partial u}{\partial y}\right)+2\dfrac{\eta_{II}}{\lambda_{II}}w_r\dfrac{\partial u}{\partial x}-\dfrac{\tau_{xx}}{\lambda_{II}}$
τ_{xx}	1	0	$-\varepsilon\left(2\tau_{yy}\dfrac{\partial v}{\partial y}+\tau_{xy}\left(\dfrac{\partial u}{\partial y}+\dfrac{\partial v}{\partial x}\right)\right)+2\left(\tau_{yy}\dfrac{\partial v}{\partial y}+\tau_{xy}\dfrac{\partial v}{\partial x}\right)+2\dfrac{\eta_{II}}{\lambda_{II}}w_r\dfrac{\partial v}{\partial y}-\dfrac{\tau_{yy}}{\lambda_{II}}$
τ_{xx}	1	0	$-\varepsilon\left(\dfrac{1}{2}(\tau_{xx}+\tau_{yy})\left(\dfrac{\partial u}{\partial y}+\dfrac{\partial v}{\partial x}\right)\right)+\left(\tau_{xx}\dfrac{\partial v}{\partial x}+\tau_{yy}\dfrac{\partial u}{\partial y}\right)+\dfrac{\eta_{II}}{\lambda_{II}}w_r\left(\dfrac{\partial u}{\partial y}+\dfrac{\partial v}{\partial x}\right)-\dfrac{\tau_{yy}}{\lambda_{II}}$

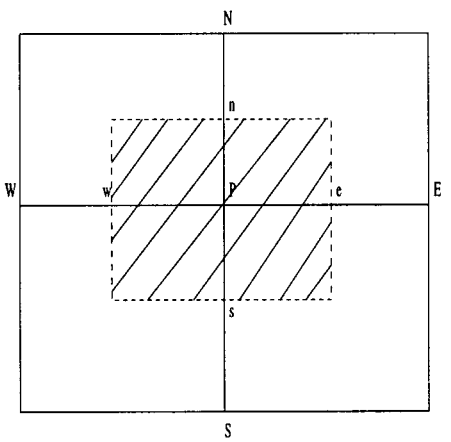

Figure 2. The control volume for grid point P.

$$\bar{S}_\Phi = \int_{\Delta V} S_\Phi \, \mathrm{d}V = \bar{S}_c + \bar{S}_P \Phi_P$$

in which $\bar{S}_c$ is the part of the $\bar{S}_\Phi$ that does not explicitly depend on Φ, and $\bar{S}_P$ is the coefficient of Φ_P that is made negative to enhance the numerical stability of the discretized equation system (2), where an overbar means that the applied values are evaluated using the known fields for iteration level n. By using a proper spatial variation approximation scheme, the final discretized equations relating the Φ_P to its neighbouring gridpoint values can be expressed symbolically in a general form in every control volume

$$a_P \Phi_P = \sum_{nb} a_{nb} \Phi_{nb} + \bar{S}_c \tag{3}$$

where

$$a_P = \sum_{nb} a_{nb} - \bar{S}_P$$

$$a_{nb} = D_{nb} f(|Pe|) + \max(\text{sign}(nb) F_{nb},\ 0)$$

where D_{nb} and Pe are the diffusion coefficient and the Peclet number respectively. $\text{sign}(nb) = +$ when $nb \in \{w, s\}$ and $\text{sign}(nb) = -$ when $nb \in \{n, e\}$. The summation is to be taken over all the neighbouring grid points nb of the central point P and the coefficients a_{nb} are the functions of the working variable, and their structures depend both on the approximation scheme used and the form of the cell. These coefficients determine the spatial accuracy of the final solution. In our calculations, the Hybrid scheme by Patankar [10] is employed to solve the momentum equations

$$f(|Pe|) = \max(0,\ 1 - 0.5|Pe|)$$

while an Upwind scheme is used in the constitutive equations for the stresses

$$f(|Pe|) = 1$$

In viscoelastic flows, the convective terms are too small in comparison with the source terms and special treatment of the source term is needed. The computation of these terms requires the first gradient of τ_{xx}, τ_{yy} and τ_{xy}. The term $\partial \tau_{xx}/\partial x$, as like as the other terms, is assuming quadratic variation of τ_{xx} along the x-direction. Thus, $\partial \tau_{xx}/\partial x$ is written as $2ax + b$.

3.1. Discretization of boundary conditions at the wall

The computation of the Neumann boundary conditions along the wall dramatically affects the solution accuracy. Second-order accuracy for the primitive variables is necessary. In this context, quadratic polynomials [17] are used to describe the velocity variations along the wall. The appropriate source term in the u-equation is defined by

$$S_u = (1 - w_r) \cdot A \cdot \left(\frac{\partial u}{\partial y} \right)_{\text{wall}} \tag{4}$$

The computation of $(\partial u/\partial y)_{\text{wall}}$ in this term is carried out assuming that u is a quadratic function of y

$$u = ay^2 + by + c \tag{5}$$

$$\frac{\partial u}{\partial y} = 2ay + b \tag{6}$$

3.2. Discretized constitutive equations

The constitutive equations are hyperbolic and we use the upwind scheme, which is stable but only ensures first-order spatial accuracy for stress. In order to attain second-order accuracy and unconditional stability, an artificial diffusion term $\nabla\cdot(\zeta\nabla\tau)$, with ζ being an artificial diffusion coefficient introduced on both sides of the constitutive equation, and discretized in the usual way. However, the current value is taken for τ on the left-hand side, while the known value, from a previous iteration level, for τ is taken on the right-hand side. In this way, the discretized constitutive equations taken the same form as Equation (3)

$$a_P\tau_P^{ij} = \sum_{nb} a_{nb}\tau_{nb}^{ij} + \bar{S}_c^{ij}$$

where the superscripts ij refer to tensor components, reserving the subscripts to the gridpoints and the overbar to values from level n. The constant part of the source term in which the stress is approximated piecewise-constantly in each control volume takes the from

$$\bar{S}_c^{xx} = \left[-\varepsilon\left(2\tau_{xx}\frac{\partial u}{\partial x} + \tau_{xy}\left(\frac{\partial u}{\partial y} + \frac{\partial v}{\partial x}\right)\right) + 2\left(\tau_{xx}\frac{\partial u}{\partial x} + \tau_{xy}\frac{\partial u}{\partial y}\right) + 2\frac{\eta_{II}}{\lambda_{II}}w_r\frac{\partial u}{\partial x}\right]\Delta V - \sum_{nb} D_{nb}\tau_P^{xx}$$

$$\bar{S}_c^{yy} = \left[-\varepsilon\left(2\tau_{yy}\frac{\partial u}{\partial y} + \tau_{xy}\left(\frac{\partial u}{\partial y} + \frac{\partial v}{\partial x}\right)\right) + 2\left(\tau_{yy}\frac{\partial u}{\partial y} + \tau_{xy}\frac{\partial v}{\partial x}\right) + 2\frac{\eta_{II}}{\lambda_{II}}w_r\frac{\partial v}{\partial y}\right]\Delta V - \sum_{nb} D_{nb}\tau_P^{yy}$$

$$\bar{S}_c^{xy} = \left[-\varepsilon\left(\frac{1}{2}(\tau_{xx} + \tau_{yy})\left(\frac{\partial u}{\partial y} + \frac{\partial v}{\partial x}\right)\right) + \left(\tau_{xx}\frac{\partial v}{\partial x} + \tau_{yy}\frac{\partial u}{\partial y}\right) + \frac{\eta_{II}}{\lambda_{II}}w_r\left(\frac{\partial u}{\partial y} + \frac{\partial v}{\partial x}\right)\right]\Delta V - \sum_{nb} D_{nb}\tau_P^{xy}$$

3.3. Solution method

The discretized equations for each control volume in the computational domain consist of a set of linear algebraic equations that can be solved easily by means of the line-by-line technique based on the Thomas algorithm or the tridiagonal matrix algorithm (TDMA) developed in Reference [10,11].

For viscoelastic fluid flow computations, the extra stress is non-linearly coupled via the source term of the momentum equations. Here, decoupled techniques can be adopted in such a way that the source term that contains the known dynamic fields obtained from the previous iteration level and the stress are updated by solving the discretized constitutive equations for obtaining the kinematics field from the momentum equations.

To obtain the kinematic fields, an equation for the pressure is obviously necessary because it is also an unknown. The strategy of pressure correction is utilized to produce the pressure equation, in which the continuity of the field is enforced via a pressure correction so that the

resulting pressure relation, which couples the pressure and the velocities, replaces the continuity relation, while the momentum equations retain their role for determining the velocity field. To avoid physically unrealistic fields, such as the checkerboard velocity and pressure distribution, staggered control volumes to be used. As shown in Figure 3, for the P-centred control volume for scalar fields, the velocities u_k $(k = x, y)$ are discretized using their values on the faces normal to the k-direction; thus, the location of the control volume for u_k in the momentum equations is staggered only in k-direction relative to the control volume for the fields (Figure 3).

The steps of present algorithm are:

*Computations of velocities.
*Computation of pressure and correction of velocities.
*Computation of stresses.
*Convergence control and return to first step if necessary.

4. NUMERICAL RESULTS

Three different meshes, depicted in Figures 4–6, have been tested in the numerical simulation. Very thin cells were required around the re-entrant section to account for the large stresses that developed in the vicinity of the corner. Table II gives the number of cells (NC), the total number of nodes (NN) as well as the area of the cells adjacent to the re-entrant corner (Area) for each grid. To test the convergence of the simulations with mesh refinement, we plot profiles of the first normal stress difference $(\tau_{xx} - \tau_{yy})$ along the centreline (Figure 7). It is clear that when compared with Mesh 2 and Mesh 3, the coarsest grid Mesh 1 allows good convergence, and we will limit the present simulations to this grid.

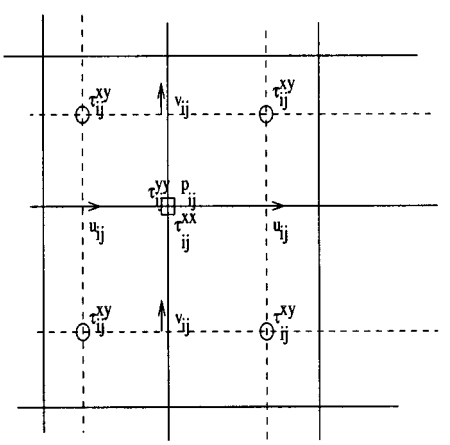

Figure 3. Two-dimensional staggered mesh and the control volumes for u, v, p well as τ.

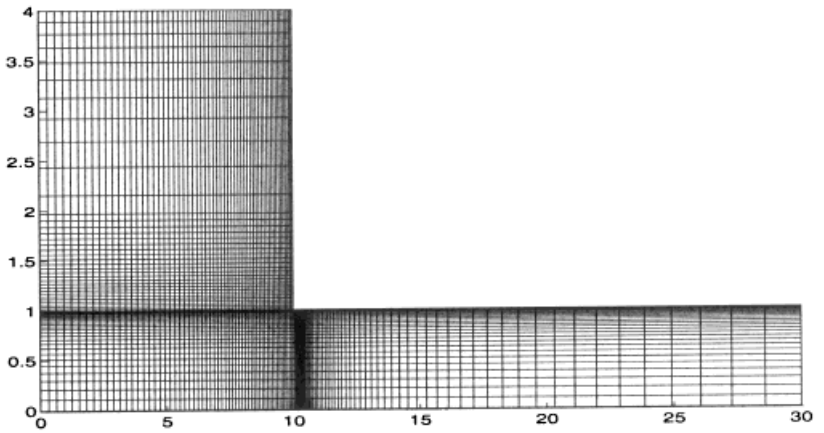

Figure 4. Mesh 1.

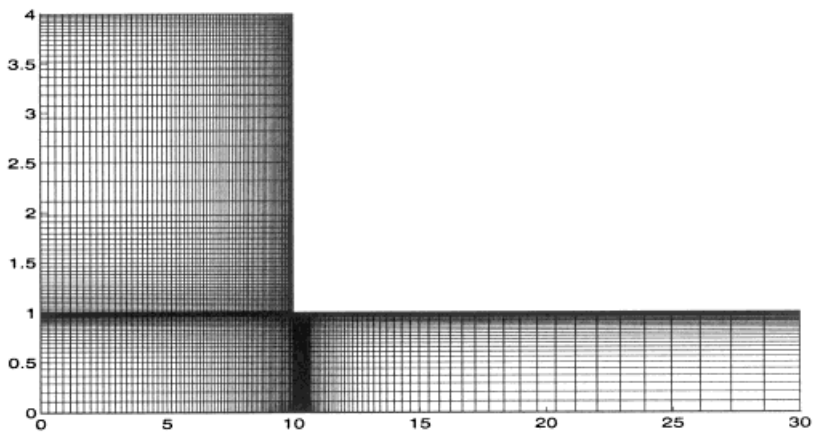

Figure 5. Mesh 2.

The flow along the centreline has an elongational nature and the elongational properties of the rheological models play an important role in determining the way it responds to the accelerating forces when it approaches the corner. Velocity profiles for Weissenberg number $We = 1$ are plotted in Figure 8. This figure shows an important velocity overshoot near the corner. Marchal and Crochet [18] have also predicted similar velocity overshoots and high stress peaks near the singular region in their high *De* calculation with Oldroyd-B fluid.

First normal stress difference profiles for different values of the Weissenberg number are reproduced in Figure 9. The maximum of $(\tau_{xx} - \tau_{yy})$ is reached just upstream of the entry section. As *We* increases, the value of this maximum increases sharply.

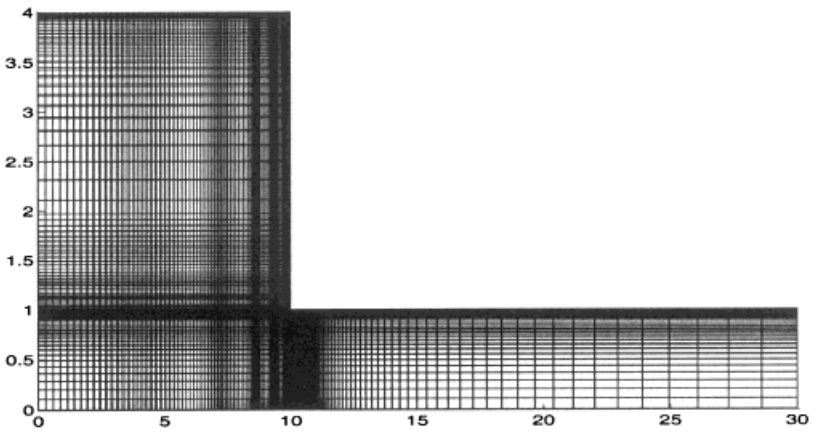

Figure 6. Mesh 3.

Table II. The number of cells (NC), number of nodes (NN) and area of the cell adjacent to the re-entrant corner.

	NN	NC	Area
Mesh 1	5075	4897	6.859E−04
Mesh 2	7532	7314	3.562E−04
Mesh 3	9118	8880	1.967E−04

Profiles of the normal extra stresses τ_{xx} and τ_{xy} are presented in Figure 10. This figure shows a high τ_{xx} and τ_{xy} peak near the corner.

In Figures 10–12 we present the extra stresses τ_{xx} and τ_{xy} for different values of ε; we show that the value of the peak of this variable increases as ε decreases.

In Figure 13, the pressure streamlines distribution is shown for $(Re,\ w_r,\ \varepsilon,\ We) = (0.01,\ 0.8,\ 0.5,\ 1)$, where the solution becomes more and more oscillatory near re-entrant corner as We increases.

In Figure 14 we present distribution of τ_{xx} and τ_{xy} for $(Re,\ w_r,\ \varepsilon,\ We) = (0.01,\ 0.8,\ 0.5,\ 1)$. It is clear that the re-entrant corner represent a singularity, many lines pass a cross this point.

5. CONCLUSION

The planar 4:1 contraction flow of White–Metzner fluid has been simulated by utilizing a finite volume method on a non-uniform staggered grid system. With the FVM, the velocity and pressure fields are made to satisfy the same momentum equation at the end of each step, and the pressure correctors are used to correct the velocity field only. To make the method

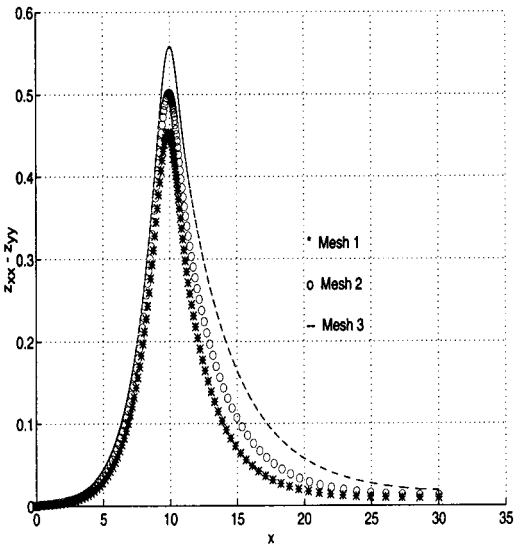

Figure 7. $(z_{xx} - z_{yy})$ on $y = 1$ of the three different meshes.

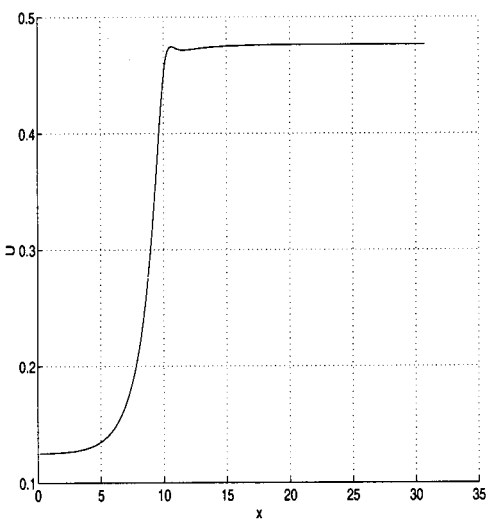

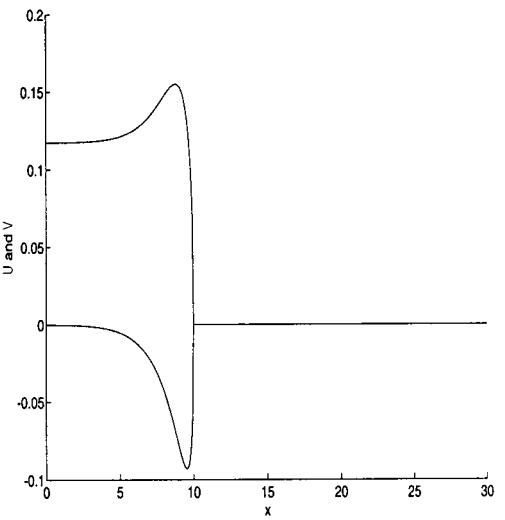

Figure 8. U and V on $y = 0$ and $y = 1$ respectively.

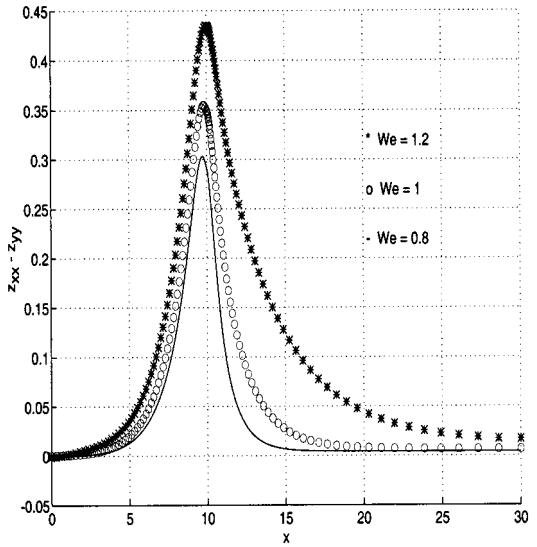

Figure 9. $(z_{xx} - z_{yy})$ on $y = 1$ for $We = 0.8$, 1 and 1.2.

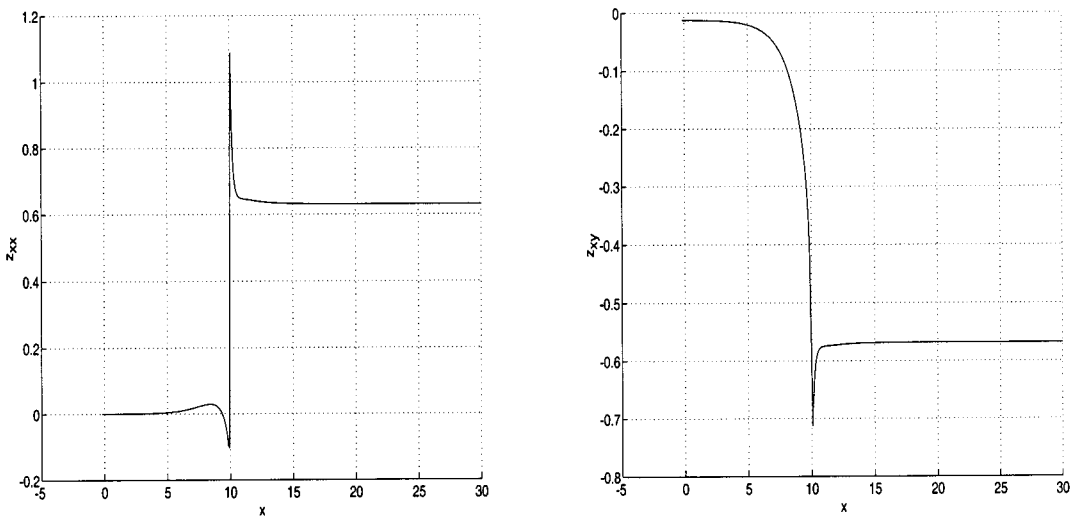

Figure 10. z_{xx} and z_{xy} on $y = 1$ respectively with $\varepsilon = 0.3$.

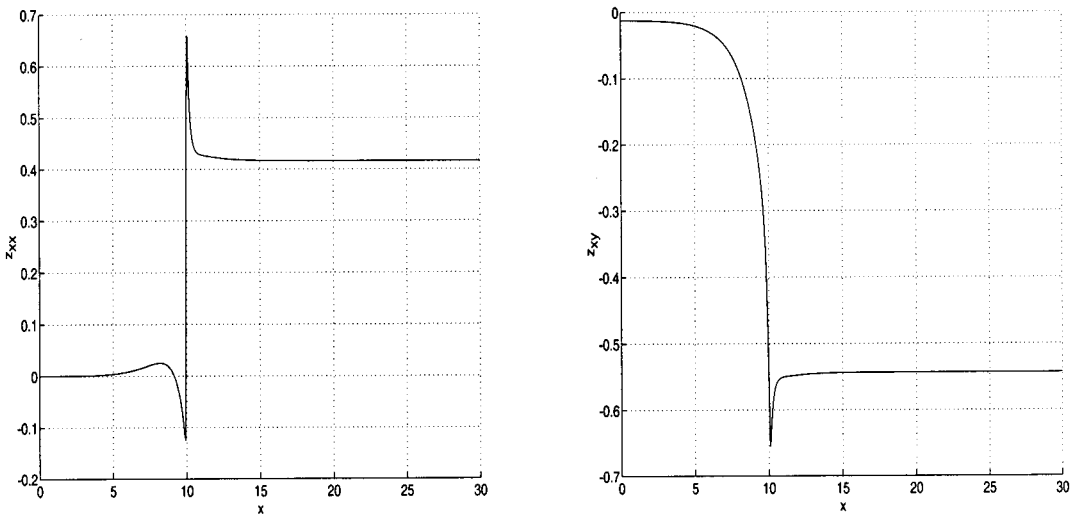

Figure 11. z_{xx} and z_{xy} on $y = 1$ respectively with $\varepsilon = 0.5$.

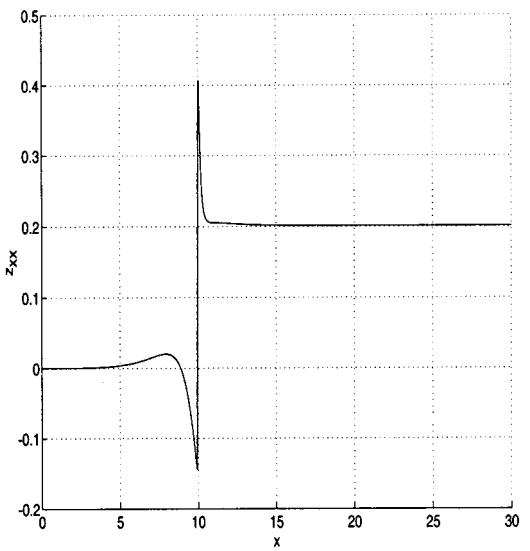

Figure 12. z_{xx} and z_{xy} on $y = 1$ respectively with $\varepsilon = 0.8$.

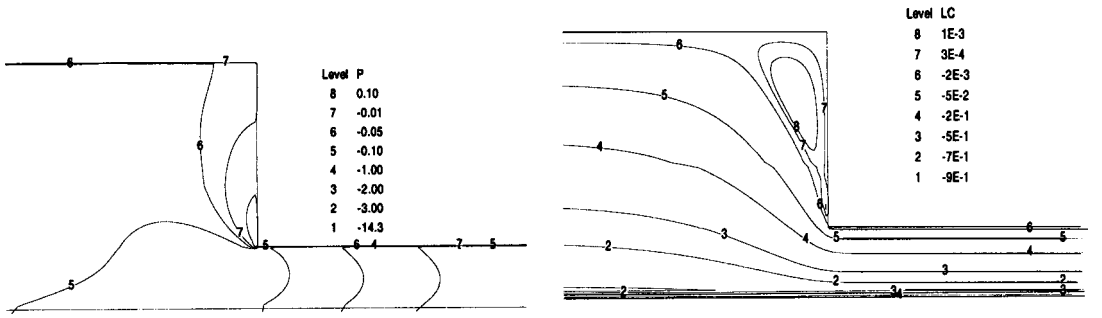

Figure 13. Isolines of pressure and streamlines respectively.

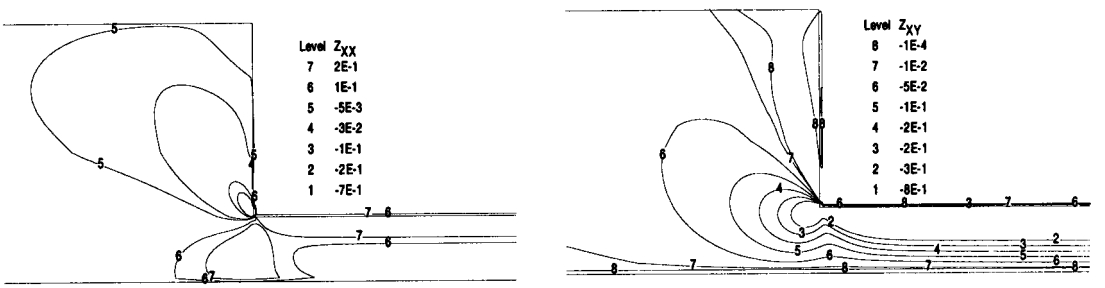

Figure 14. Isolines of z_{xx} and z_{xy} respectively.

suitable for viscoelastic flow computations, decoupled techniques are employed and artificial diffusion terms are introduced on both sides of the discretized constitutive equations to stabilize the numerical calculation. With the method, thanks to the modest demand on memory, it becomes possible to solve large problems on small computer systems.

As a results, the present numerical simulation has allowed us to reproduce much of the experimental results.

REFERENCES

1. Crochet MJ, Pilate G. Plane flow of a fluid of second grade through a contraction. *Journal of Non-Newtonian Fluid Mechanics* 1976; **1**: 247–258.
2. Perera MGN, Walters K. Long-range memory effects in flows involving abrupt changes in geometry. Part I. Flows associated with L-shaped and T-shaped geometries. *Journal of Non-Newtonian Fluid Mechanics* 1977; **2**: 49–81.
3. Perera MGN, Walters K. Long-range memory effects in flows involving abrupt changes in geometry. Part II. The expansion–contraction–expansion problem. *Journal of Non-Newtonian Fluid Mechanics* 1977; **2**: 191–204.
4. Crochet MJ, Davies AR, Walters K. *Numerical Simulation of Non-Newtonian Flow*. Elsevier: Amsterdam, 1984.
5. Beris AN, Armstrong RC, Brown RA. Spectral/finite element calculations of the flow of a Maxwell fluid between eccentric rotating cylinders. *Journal of Non-Newtonian Fluid Mechanics* 1987; **22**: 129–167.

6. Boger DV. Viscoelastic flows through contractions. *Annual Review in Fluid Mechanics* 1987; **19**: 157–182.
7. Mitsoulis E. Numerical simulation of viscoelastic fluids. In *Encyclopedia of Fluid Mechanics*, *vol. 9*, *Polymer Flow Engineering*, Cheremisinoff NP (ed.). Gulf Publishing: Dallas, TX, 1990; 649–704.
8. Maders H, Vergnes B, Demayand Y, Agassant JF. Steady flow of a White–Metzner type. *Journal of Mathematical Analysis and Application* 1992; **45**: 63–80.
9. Hakim A. Mathematical analysis of viscoelastic fluids of White–Metzner type. *Journal of Mathematical Analysis and Application* 1994; **185**(3): 675–705.
10. Patankar SV. *Numerical Heat Transfer and Fluid Flow*. McGraw-Hill: New York, 1980.
11. Van Doormaal JP, Raithby GD. Enhancement of the SIMPLE method for preciding incompressible fluid flows. *Numerical Heat Transfer* 1984; **7**: 147–163.
12. Hu HH, Joseph DD. Numerical simulation of viscoelastic flow past a cylinder. *Journal of Non-Newtonian Fluid Mechanics* 1990; **37**: 347–377.
13. Yoo JY, Na Y. A numerical study of the planar contraction flow of a viscoelastic fluid using SIMPLER algorithm. *Journal of Non-Newtonian Fluid Mechanics* 1991; **39**: 89–106.
14. Darwish MS, Whiteman JR, Beris MJ. Numerical modelling of viscoelastic liquids using a finite-volume method. *Journal of Non-Newtonian Fluid Mechanics* 1992; **45**: 311–337.
15. Sasmal GP. A finite volume approach for calculation of viscoelastic flow through an abrupt axisymmetric contraction. *Journal of Non-Newtonian Fluid Mechanics* 1995; **47**: 15–47.
16. Phan-Thien S-CN, Tanner RI. Numerical study of secondary flows of viscoelastic fluid in straight pipe by an implicit finite volume method. *Journal of Non-Newtonian Fluid Mechanics* 1995; **59**: 191–213.
17. Anderson DA, Tannehill JC, Pletcher RH. *Computational Fluid Mechanics and Heat Transfer*. McGraw-Hill: New York, 1984; 57–61.
18. Marchal JM, Crochet MJ. A new mixed finite element for calculating viscoelastic flow. *Journal of Non-Newtonian Fluid Mechanics* 1987; **26**: 77–114.

